High-fidelity modeling of a vertical axis tidal turbine model under realistic flow conditions

Mikaël Grondeau and Sylvain Guillou

Abstract—**It is now well known that turbulence has an influence over tidal turbines performances and wake. Turbulence is a complex phenomenon that can be quantified using advanced statistics such as the average velocity, the Reynolds tensor and the integral turbulence length scale.**

In-situ measurements made at tidal sites have shown that turbulent flow can have various values for these parameters and it is thus important to predict their effects over turbines. In this paper, the influence of turbulence length scales is studied using an unsteady Computational Fluid Dynamics approach based on the Lattice Boltzmann Method and the Actuator Line Method. The tidal turbine is a $1/20^{th}$ model of the HydroQuest® Vertical Axis Tidal Turbine.

The model is first validated by comparing numerical results with experimental ones. The ALM-LBM-LES model is found to be accurate for predicting the average velocity and average velocity fluctuations in the wake in flood tide configuration. Three scenarios with different turbulence length scales are then analyzed. It is observed that a larger integral length scale leads to larger velocity fluctuations in the wake.

Index Terms—**Tidal Turbine, Turbulence, Computational Fluid Dynamics, Lattice Boltzmann Method.**

I. Introduction

In the context of the global energy crisis, developing renewable energies is of primal importance. Among the renewable resources available are tidal currents. Tidal currents can be exploited with tidal turbines. Different concepts of tidal turbine exist, a Vertical Axis Tidal Turbine (VATT) prototype made by HydroQuest® and CMN® is examined here. More precisely, numerical investigations on a HydroQuest® tidal turbine model are realized.

Most tidal sites are characterized by having strong turbulence intensities [1]. The presence of turbulence in most tidal sites has led companies and academics to study the effects of ambient turbulence over tidal turbines. It has been shown that turbulence can have a significant influence on the turbine performances and wake [2]. More precisely, the influence of the integral length scale of the turbulence is still not fully understood [3], even though it varies significantly inside a single tidal site [4].

This work is currently funded by the European Union in the form of the FCE INTERREG TIGER Project

Mikaël Grondeau is with the LUSAC laboratory of the University of Caen, 60 rue Max-Pol Fouchet, CS 20082, 50130 Cherbourg-en-Cotentin, France (email: mikael.grondeau@unicaen.fr)

Sylvain Guillou is with the LUSAC laboratory of the University of Caen, 60 rue Max-Pol Fouchet, CS 20082, 50130 Cherbourg-en-Cotentin, France (email: sylvain.guillou@unicaen.fr)

Digital Object Identifier:
https://doi.org/10.36688/ewtec-2023-218

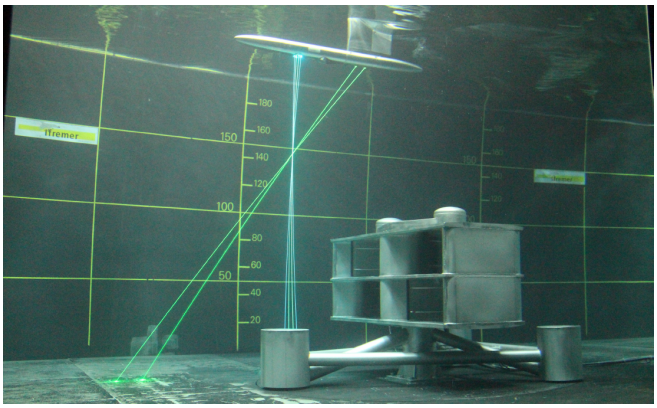

Fig. 1. Tidal turbine model of the HydroQuest® VATT tested at Ifremer's testing facility [9].

Given the size of tidal turbines, experimental studies have to scale down turbines, keeping the Froud similarity but not the Reynolds similarity. The Reynolds number is then often not high enough to reach Reynolds convergence, and the blades behave differently from those of the full-size device. In situ measurement are still expensive and difficult to acquire. Computational Fluid Dynamics (CFD) is an interesting complementary approach to experiments. Because the hydrodynamic of vertical axis tidal turbines is highly unsteady, Large Eddy Simulation (LES) are well adapted here.

Blade-resolved Computational Fluid Dynamics (CFD) approaches are appropriate to study vertical axis tidal turbines, but their cost is still prohibitive for real size tidal turbine [5]. Simplified approaches are preferred solutions. Shamsoddin and Porté-Agel (2014) [6] showed that Actuator Line Model (ALM) LES is well suited to model vertical axis turbine. Although more demanding in terms of computational resources than the Actuator Cylinder, the ALM is better suited for studying the wake of a single turbine.

The Lattice Boltzmann Method (LBM) is an unsteady weakly-compressible CFD approach [7]. It solves the Boltzmann equation using an explicit time discretization and a uniform Cartesian grid called lattice. It has been proven to be an efficient approach for modeling tidal turbines using LES and ALM [8].

In this paper, a tidal turbine model of the HydroQuest® VATT is studied using an ALM-LBM-LES approach. This model was tested at the Ifremer Boulogne-sur-Mer testing facilities, [9]. After a presentation of the models used, numerical results are compared with experimental ones in a scenario where the turbine is placed within a turbulent boundary layer and is in a flood tide configuration. A numerical

investigation of the influence of upstream turbulence length scales on the turbine wake is then realized.

II. Methods

The CFD tool used for this work consists of a combination of several models that are briefly presented here. The Actuator Line Model is first presented. The Lattice Boltzmann Method is then presented along with some of the implementation specific to the context of this study. This section ends with a short presentation of the Synthetic Eddy Method used for generating a realistic Turbulent Inflow Condition.

A. Actuator Line Model

The Actuator Line Model is a simplified approach to the modeling of tidal turbines blades. The method was first and mostly applied to wind turbines. The main concept is to replace the actual blade with a line made of several elements. Each of these elements apply a force to the fluid surrounding it. The action of the force is supposed to model the action of the blade on the fluid. Its calculation has a massive influence on how accurate the model is and requires a particular attention [10]. The other parameters are the spacing between the actuator line elements and the kernel used to spread the force onto the mesh/lattice.

The force is calculated from the tabulated lift and drag coefficients of the blade profile. These coefficients are calculated using the XFLR5 software. The profiles are NACA 0018 projected onto the swept cylinder of radius 0.2 m. The blade is transformed using the virtual camber transformation correction for TSR = 1.6.

$$\eta(\epsilon, d) = \frac{1}{\epsilon^3 \pi^{1.5}} \exp\left(-\left(\frac{d}{\epsilon}\right)^2\right) \tag{1}$$

At each time iteration of the simulation, the angle of attack is calculated using the velocity of the fluid interpolated at the elements location. The interpolation is made with the same kernel as the one used for the force and is described in Equation 1, where ϵ is the regularization parameter of the kernel and d is the distance from the line element to a fluid node. Due to the chosen implementation, the regularization parameter ϵ is equal to $2\Delta x_{ALM}$, where Δx_{ALM} is the grid spacing at the turbine location. Once the coefficients have been picked up from the tabulated C_L and C_D, the force is calculated using the relative velocity of each elements.

To account for the dynamic stall of the blade during rotation, the MIT dynamic stall model has been implemented in the ALM algorithm. It is described in detail in the appendix of [11].

B. The Lattice Boltzmann Method

The Lattice Boltzmann Method is an unsteady CFD method based on the Boltzmann equation for fluid flows. It's a mesoscopic representation of the collision between fluid molecules. The ALM approach has been implemented in the Palabos [12] open-source LBM library for the easy access to an efficient parallel LBM solver it provides.

The LBM is solved using an explicit time discretization on a uniform Cartesian lattice. Palabos has a multi-level lattices feature. It allows the numerical domain to be split into lattices with different grid-spacing, thus increasing resolution in areas of major interest. The grid spacing between two adjacent levels must be of a factor 2.

One specificity of the LBM is the discretization of the velocity space over which molecules propagate. Indeed the Boltzmann equation is a function of time, space and velocity. The velocity space is thus restricted to a finite number of directions. A scheme with 19 directions is employed.

The core of the LBM is the collision model. It dictates the stability, accuracy and physics of the method. The context here is a low Mach, high Reynolds number and single phase fluid flow. A suitable collision model for this type of flow is the Regularized Single-Relaxation-Time BGK collision described in [13].

In order to save computational resources, the small turbulent structures are modeled with a Large Eddy Simulation model. This model is the static Smagorinsky model of Malaspinas and Sagaut (2012) [14] that is already available in the Palabos library.

C. The Synthetic Eddy Method

This paper focuses on the influence of turbulence integral length scales over the turbine wake. It is thus essential to generate an turbulent upstream flow realistic enough. For this purpose, the Synthetic Eddy Method (SEM) of Poletto *et al.* (2013) [15] is used. This technique has already proven its accuracy several times with an LBM-LES approach [8] [16] [17].

The implemented SEM creates a random superimposition of coherent turbulent structures. These artificial vortices are located in a box encapsulating the inlet and are advected with the mean flow. Once they reach the end of the box, they are recycled.

Vortices have several adjustable parameters. The parameter of interest in this study is the radius of the vortices, which prescribes the integral scale of the generated turbulence. It has been shown in Grondeau *et al.* (2022) [17] that vortices radius prescribes the integral length scale of the turbulence. Integral length scale was measured using spatial auto-correlation at several locations downstream of the inlet. The SEM used here is set to generates an isotropic turbulence. The Reynolds tensor can also be prescribed to match a certain turbulence intensity profile. The last parameter is the number of vortices. It is chosen in order to have a theoretical coverage of the inlet of at least 100 %.

A vortex only influences the inlet nodes within its radius. The velocity of an inlet node is calculated by adding the contribution of every vortices affecting it.

III. Simulations setup

This section presents the setups of the numerical model. Configurations in which the tidal turbine have

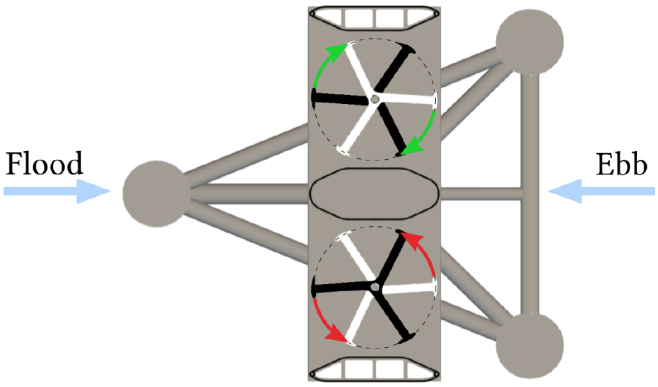

Fig. 2. Top view of the turbine model of the HydroQuest® VATT tested at Ifremer's testing facility with Flood and Ebb tide configurations [9].

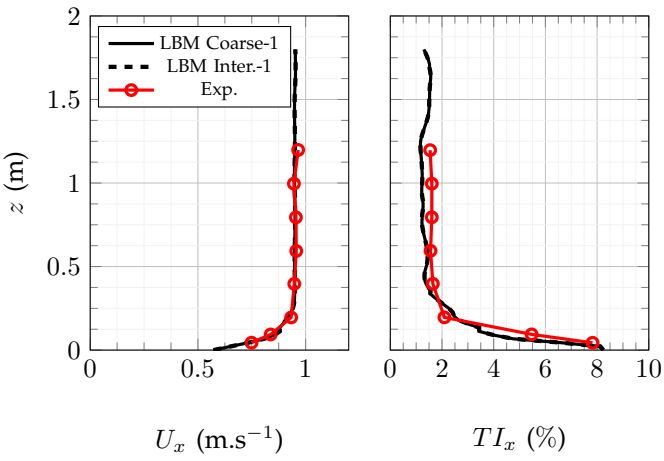

Fig. 3. Average axial velocity and turbulence intensity taken 3 m upstream of the turbine of ALM-LBM-LES simulations. Average axial velocity and turbulence intensity from the experiment of Moreau *et al.* (2022) [9]

been studied are first exposed. The 4 different Turbulent Inflow Conditions of the SEM are then listed. Finally, a mesh dependence analysis validates the numerical domain used for the turbulence analysis. Numerical results are also confronted with experimental ones.

A. The turbine

The turbine modeled is a $1/20^{\text{th}}$ HydroQuest® model that was tested at Ifremer's flume tank in Boulogne-sur-Mer [9], Figure 1. It's a four rotor turbine, each rotor has three blades. The rotor radius is $R = 0.2$ m. The overall height of the model from the floor to the top is 0.84 m. The top and bottom rotors are shifted by an angle of 60 degrees.

The blades are modeled with the ALM presented in Section II-A. The spacing between each line elements is $0.5\ \Delta x_{ALM}$, where Δx_{ALM} is the mesh size at the turbine location.

The turbine fairings and gravity base geometries are entirely resolved. Since the boundary layer around the non-moving parts is going to be under resolved, a boundary layer model is used to improve the accuracy. It is based on the Musker profile [18] for imposing the tangent-wall velocity and imposes a zero wall-normal velocity. The pressure is interpolated from the fluid nodes contacting the wall node.

Moreau *et al.* (2023) [9] studied two turbine configurations called ebb and flood, Figure 2. Only the flood configuration is considered in this paper. The turbine operates at $TSR = 1.6$ and the upstream flow velocity is $U_0 = 0.95$ m.s^{-1}.

B. Upstream turbulence and boundary conditions

The upstream turbulence is generated using the SEM presented in Section II-C. Four Turbulent Inflow Conditions (TIC) are studied, numerated from 0 to 3. TIC No. 0 is the turbulent boundary layer of the experiment [9]. It is used for comparing the numerical and experimental results in Section III-C. The average axial velocity and turbulence intensity profiles are given in the reference paper of Moreau *et al.* (2022) [9]. They are used to calibrate the SEM. The radius of the SEM vortices is 0.25 m and there are 200 vortices.

TABLE I
SYNTHETIC EDDY METHOD TURBULENT INFLOW CONDITIONS USED IN THE SIMULATIONS.

TIC No.	Turb. Intensity	Vortices number	Vortices radius
0	Experiment	200	0.25 m
1	10 %	200	0.33 m
2	10 %	200	0.66 m
3	10 %	200	0.99 m

A comparison between the experimental profiles and the numerical profiles 3 m upstream of the turbine is given in Figure 3. An excellent fit is observed. The other three TIC have the same average velocity profile as TIC No. 0 and a constant turbulence intensity from the tank floor to the surface. Table I summarizes the four TIC parameters. The turbulence intensity is defined as T.I. $= 100\sqrt{u_x u_x}/U_x$, where $u_x u_x$ are the average axial velocity fluctuations and U_x the average axial velocity.

The bottom and sides boundary conditions impose a tangential velocity calculated from the Musker boundary layer profile. The top boundary condition is a free-slip boundary condition. The outlet of the domain imposes a constant pressure and has a wave absorbing layer of 2 m on top of it [19]. The numerical domain is 20 m long, 2 m tall and 4 m wide. These are the exact dimensions of the testing facilities used in [9] and the blockage ratio is of 12 %. Since no blockage ratio corrections were used in [9], they are not applied here.

C. Accuracy and mesh sensitivity

To validate the approach, meshes with 3 different ALM mesh sizes Δx_{ALM} have been selected. All meshes have 3 levels. There are 6 configurations in total, two coarses, two intermediates and one fine. The additional coarse and intermediate configurations have a longer fine level. All configurations are summarized in Table II. The mesh of configuration Coarse-1 can be seen on Figure 4, the mesh of configuration Intermediate-2 on Figure 5 and the mesh of Fine-1 on Figure 6. The 3-dimensional wake predicted with

TABLE II
CONFIGURATIONS STUDIED FOR THE VALIDATION OF THE ALM-LBM-LES APPROACH.

Config.	Δx_{ALM} (m)	D_I (m)	Nodes	h.CPU (h)
Coarse-1	$1.25 \cdot 10^{-2}$	1	$12.3 \cdot 10^6$	677
Coarse-2	$1.25 \cdot 10^{-2}$	2	$13.2 \cdot 10^6$	825
Inter.-1	$6.25 \cdot 10^{-3}$	0.75	$37.0 \cdot 10^6$	5129
Inter.-2	$6.25 \cdot 10^{-3}$	2	$44.2 \cdot 10^6$	8547
Fine.-1	$4.17 \cdot 10^{-3}$	0.75	$124.7 \cdot 10^6$	14007

D_I is the distance between the turbine and the first downstream level interface.
Nodes is the total number of nodes in the mesh.
h.CPU is the wall-clock simulation time multiplied by the number of CPU.

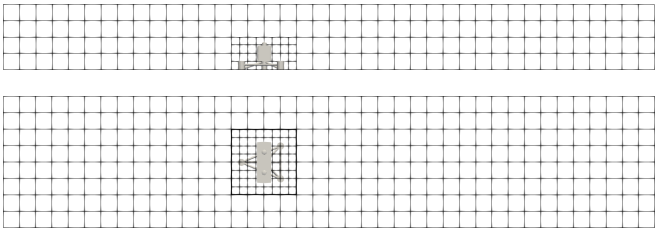

Fig. 4. Configuration Coarse-1. Mesh in cuboids of $20 \times 20 \times 20$ nodes.

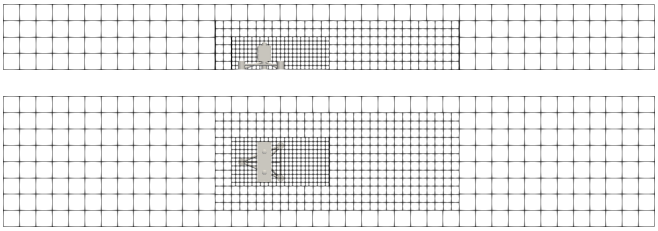

Fig. 5. Configuration Intermediate-2. Mesh in cuboids of $20 \times 20 \times 20$ nodes.

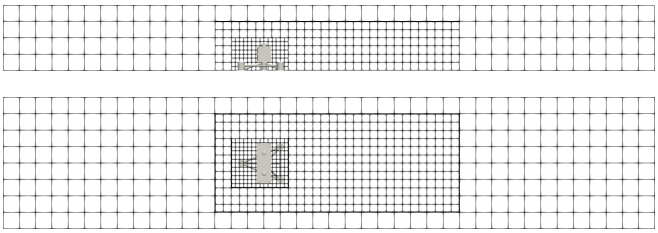

Fig. 6. Configuration Fine-1. Mesh in cuboids of $30 \times 30 \times 30$ nodes.

the ALM-LBM-LES approach with configuration Inter.-2 can be seen in Figure 7. Simulations are run for 26 s of simulated time before statistics are computed. Statistics are then computed over another 26 s. This corresponds to 32 revolutions of the turbine.

Numerical results from Coarse-1, Inter.-1 and Fine-1 configurations are compared to experimental results from Moreau *et al.* (2022) [9]. Data are plotted at several distances downstream of the turbine and at two locations in the span-wise y direction. The span-wise locations are the turbine center-line ($y = 0$) and the center of the right-hand rotors ($y = 0.31$ m).

Figure 8 and 9 plot the average axial velocity profiles at $x = 0.9$ m and $x = 4.05$ m downstream of the turbine. There is a significant gap in accuracy between the Coarse-1 configuration and the Inter.-1 and Fine-1

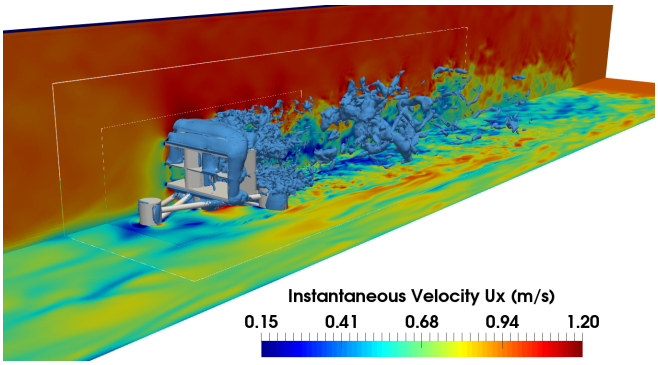

Fig. 7. Tidal turbine model of the HydroQuest® VATT modeled with ALM-LBM-LES using configuration Inter.-2. Iso-contour of the instantaneous pressure field and slices of the instantaneous axial velocity field.

configurations. For $y = 0.31$ m, predictions made with Inter.-1 configuration are slightly better than with Fine-1. The opposite is observed at $y = 0$ m. Average axial velocity fluctuations $\sqrt{u_x u_x}$ are plotted on Figure 10 and 11. Results from Coarse-1 are significantly further away from the reference than Inter.-1 and Fine-1 results. Fluctuations are slightly over-estimated in the far wake by all configurations.

The ALM-LBM-LES approach has three grid-dependent models: the LES model, the boundary layer model and the ALM model. In Section II-C, it has been shown that the velocity and turbulence profiles generated by the SEM upstream of the turbine, where the mesh is the coarsest, were accurate. The LES model is thus well suited for the coarsest mesh as well as for the finer ones.

The dimensionless mesh size Δx^+ around the turbine is close to 1000 for the Coarse-1 configuration. This rather large Δx^+ could be outside of the logarithmic region of the turbulent boundary layer and decrease the accuracy of the turbine boundary condition significantly. On the other hand, the Δx^+ for the Inter.-1 and Fine-1 likely falls within the turbulent boundary layer.

As explained in Section II-A, the regularization parameter of the kernel ϵ is linked to the mesh size Δx_{ALM} in the current implementation. However, it has been shown that there are optimal values for this parameter based on the airfoil chord c. According to [20], optimal values for this parameter should be comprised within $[0.1c, 0.25c]$. Table III summarizes ϵ values for configurations Coarse, Inter. and Fine. The only configurations with a relaxation parameter outside of the recommended range are Coarse-1 and Coarse-2.

Based on these observations and the results of Figures 8 9 10 11, configuration Coarse-1 is likely too coarse for the present study. Meshes Inter.-1 and Fine-1 have accurate enough predictions. In order to reduce computational costs, only configuration Inter.-1 is considered for further study.

To estimate the influence of the mesh interface placed immediately after the turbine in configurations Coarse-1 and Inter.-1, two additional simulations are run with configurations Coarse-2 and Inter.-2. A comparison between these 4 configurations is made in Figure 12.

TABLE III
RELAXATION PARAMETER ϵ OF THE FORCE KERNEL IN CONFIGURATIONS COARSE, INTER. AND FINE.

Config.	ϵ/c	$\in [0.1c, 0.25c]$
Coarse-1	0.34	No (+36%)
Coarse-2	0.34	No (+36%)
Inter.-1	0.17	Yes
Inter.-2	0.17	Yes
Fine.-1	0.11	Yes

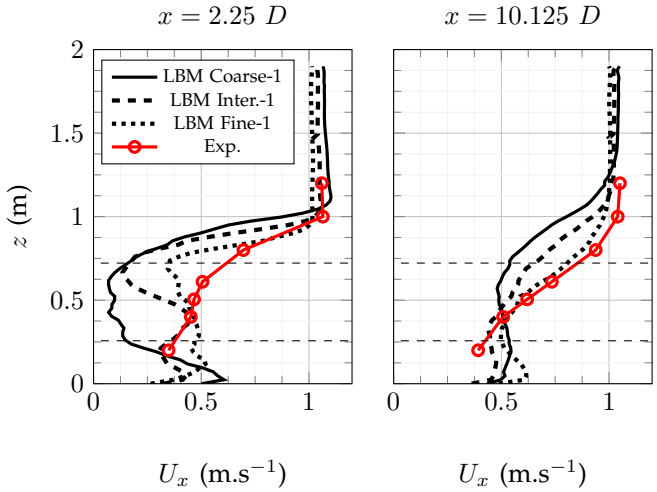

Fig. 8. Average axial velocity U_x at $x = 2.25\ D$ and $10.125\ D$ downstream of the turbine. Profiles located at $y = 0$ m.

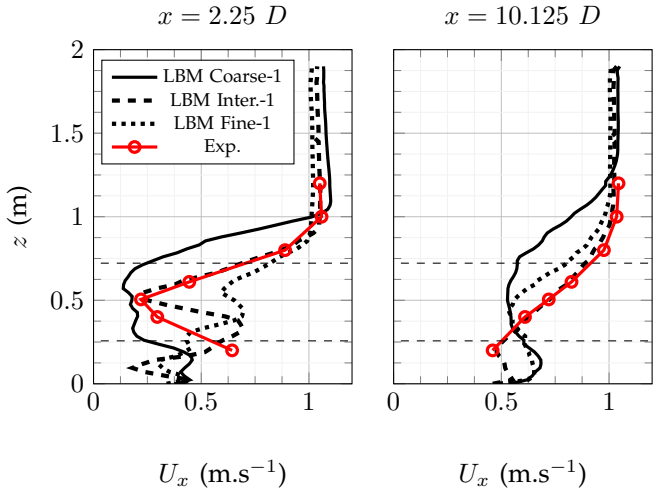

Fig. 9. Average axial velocity U_x at $x = 2.25\ D$ and $10.125\ D$ downstream of the turbine. Profiles located at $y = 0.31$ m.

Results are almost identical at $x = 0.9$ m between cases 1 and 2. At $x = 4.05$ m downstream, differences are observed between configurations Coarse-1 and Coarse-2, highlighting an influence of the interface. No influence is observed between configurations Inter.-1 and Inter.-2. To save computational cost, configuration Inter.-1 is chosen over Inter.-2 for the rest of the study.

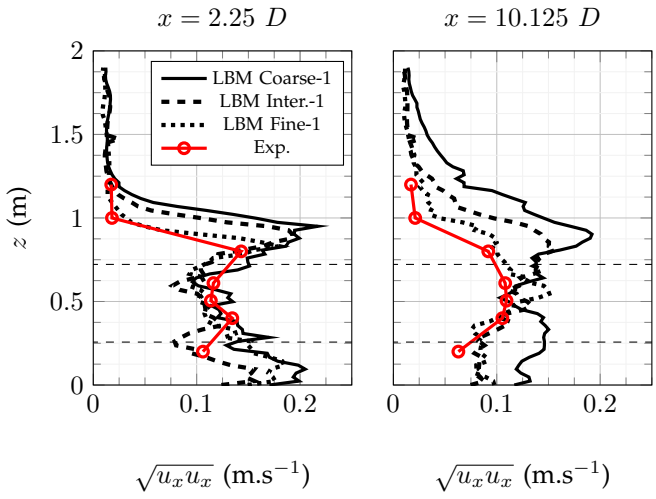

Fig. 10. Average velocity fluctuations $\sqrt{u_x u_x}$ at $x = 2.25\ D$ and $10.125\ D$ downstream of the turbine. Profiles located at $y = 0$ m.

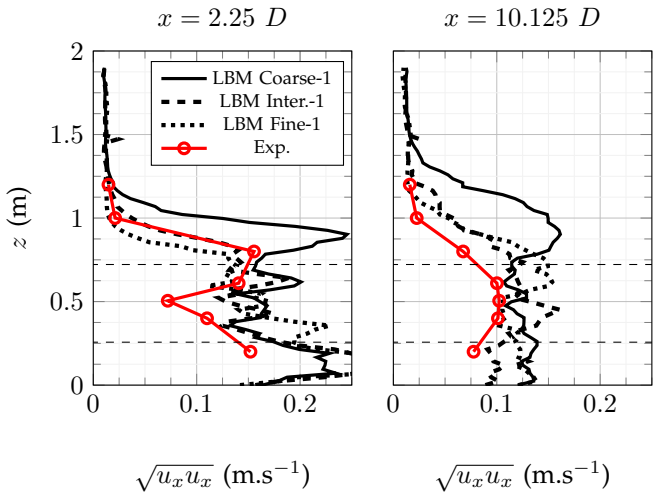

Fig. 11. Average velocity fluctuations $\sqrt{u_x u_x}$ at $x = 2.25\ D$ and $10.125\ D$ downstream of the turbine. Profiles located at $y = 0.31$ m.

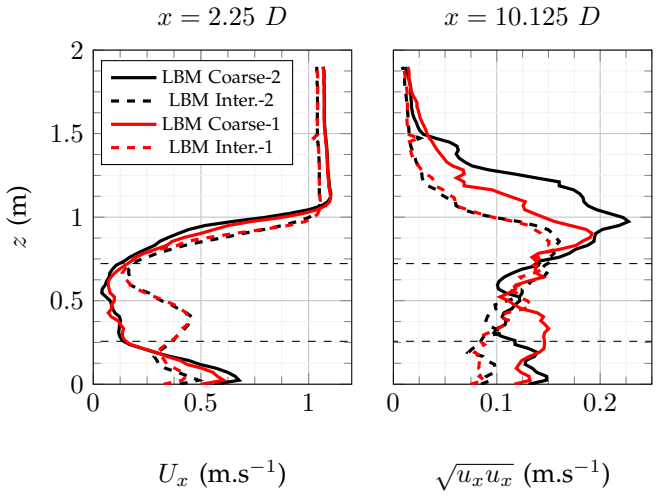

Fig. 12. Average axial velocity U_x and average velocity fluctuations $\sqrt{u_x u_x}$ for configurations Coarse-1 and 2 and Inter.-1 and 2. Profiles located at $y = 0$ m.

IV. Influence of turbulence length scale

The influence of 3 Turbulent Inflow Conditions on the turbine wake is evaluated in this section. Their parameters are summarized in Table I. The only characteristic of the turbulent flow that varies between these configurations is the length scale of the turbulent structures with $L = [0.33, 0.66, 0.99]$ m. The wake expansion is first looked at, then the turbulence induced by the turbine.

A. Wake expansion

To visualize the wake expansion, iso-contours of the average axial velocity field in x-y slices at the top-rotors mid-height are plotted. These plots can be seen on Figure 13. It is observed that although the turbulence rate is the same, the shape of the iso-contours are quite different between the 3 cases. Case with TIC No. 1 has the wider far wake with an iso-contour at $U_x = 0.8$ m.s^{-1} dividing into three branches. For TIC No. 3, the far wake has merged into a single branch and doesn't expand as much as TIC No. 1 in the y direction. The trend is coherent for TIC No. 2 as it sits in between TIC No. 1 and TIC No. 3. Far wake for TIC No. 2 also divides into three branches. The close wake is relatively similar for all three TIC. The wake of the turbine with TIC No. 2 is slightly asymmetrical. This most likely comes from a too short sampling time combined with SEM vortices that are not as equally distributed as for TIC No. 1 and 3.

A x-z slice of the average axial velocity fields at $y = 0$ m is plotted on Figure 14. Looking at the iso-contour of $U_x = 0.5$ m.s^{-1}, the velocity deficit close to the turbine is more rapidly recovered for TIC No. 3 than for TIC No. 1 and 2. The iso-contour of $U_x = 0.8$ m.s^{-1} seems to indicate that the vertical expansion of the wake is greater for TIC No.3 than for TIC No. 1 and 2. The merging of the 3 branches of the far wake into 1 for TIC No. 3, observed in Figure 13, is probably the cause of this change in shape. A larger turbulence length scale therefore concentrates the wake closer to the turbine center-line at $y = 0$ m.

B. Turbine induced turbulence

Averaged profiles of the stream-wise velocity fluctuations for TIC No. 1 2 3 at $x = 0.9$ m and 4.05 m downstream of the turbine are plotted on Figure 15 for $y = 0$ m and on Figure 16 for $y = 0.31$ m. At $y = 0.0$ m, an influence of the TIC is observed on both profiles. Fluctuations seem to be larger for TIC No. 3 than for TIC No. 2 and TIC No. 1, especially at $x = 4.05$ m. At $y = 0.31$ m, the trend is less noticeable but still present on both profiles. This would indicate that bigger turbulent structures lead to larger velocity fluctuations in the wake of the turbine. Observations made in the previous section are coherent with this since a larger turbulence intensity leads to a greater mixing in the wake and thus a more rapidly recovered velocity deficit.

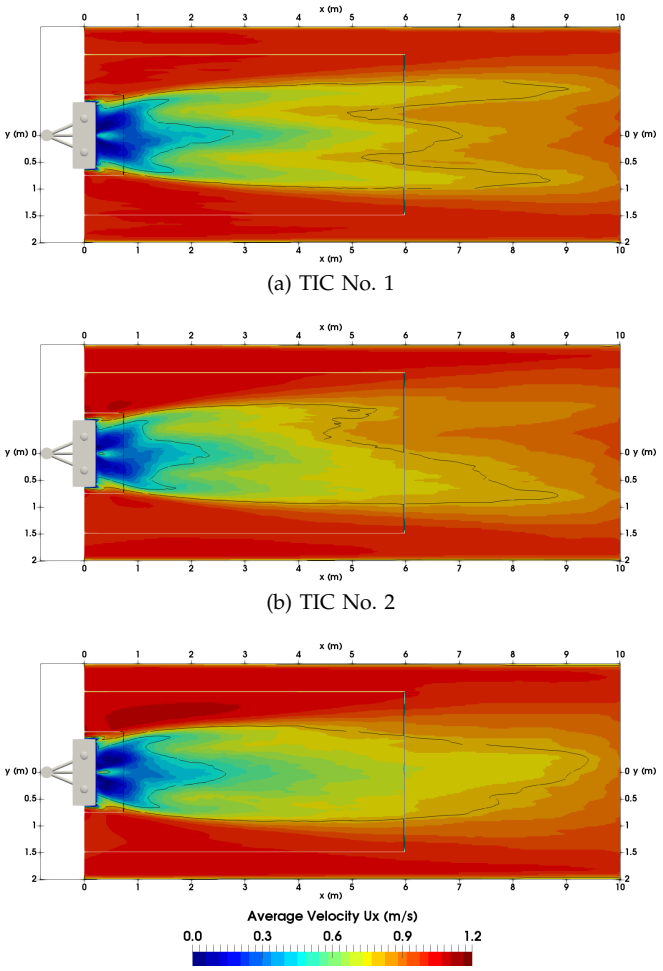

(a) TIC No. 1

(b) TIC No. 2

(c) TIC No. 3

Fig. 13. LBM simulations of the HydroQuest® turbine model with 3 different Turbulent Inflow Conditions. Average axial velocity slices at the turbine top-rotors mid-height. Iso-contour of $U_x = 0.5$ m.s^{-1} and $U_x = 0.8$ m.s^{-1}. The absorbing layer has been cut off.

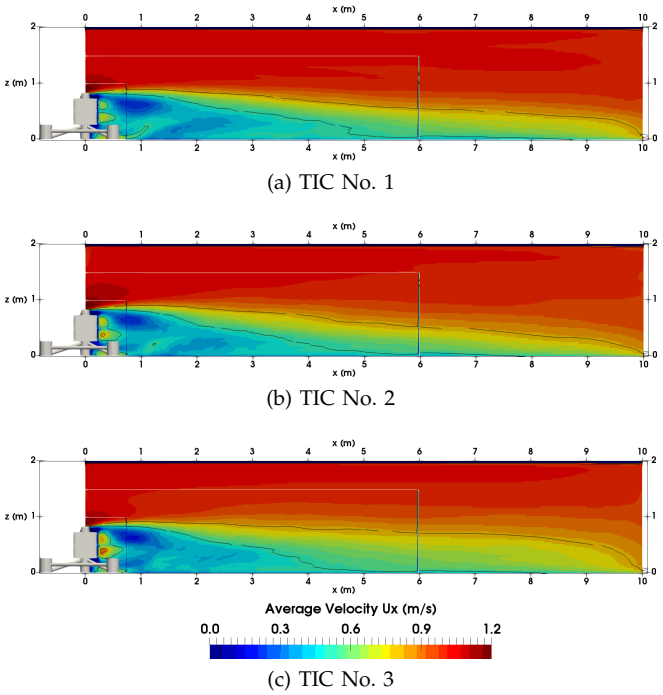

(a) TIC No. 1

(b) TIC No. 2

(c) TIC No. 3

Fig. 14. LBM simulations of the HydroQuest® turbine model with 3 different Turbulent Inflow Conditions. Average axial velocity slices at $y = 0$ m. Iso-contour of $U_x = 0.5$ m.s^{-1} and $U_x = 0.8$ m.s^{-1}. The absorbing layer has been cut off.

V. Conclusion and Prospects

The ALM-LBM-LES approach was first compared with experimental results. Numerical predictions for the average velocity and averaged velocity fluctuations were found to be accurate. After a mesh sensitivity analysis, an optimal mesh was selected for the study of the integral length scales influence over the wake of the turbine.

Three different turbulence length scales were imposed thanks to the SEM inlet boundary condition. The prescribed turbulence rate was constant and equal to 10 %. It was observed that the wake is affected by the turbulence integral length scale. Larger integral length scales led to a better velocity recovery in the close wake and overall larger velocity fluctuations in the whole wake region. The shape of the wake was also influenced, vertical expansion appeared to be strengthened by larger turbulent structures while the opposite is observed for span-wise expansion.

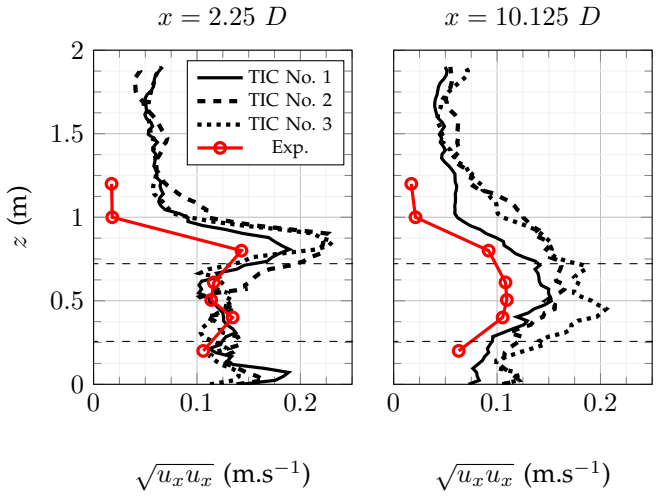

Fig. 15. Average velocity fluctuations $\sqrt{u_x u_x}$ at $x = 2.25\ D$ and $10.125\ D$ downstream of the turbine. SEM used with TIC No. 1,2,3. Profiles are located at $y = 0$ m.

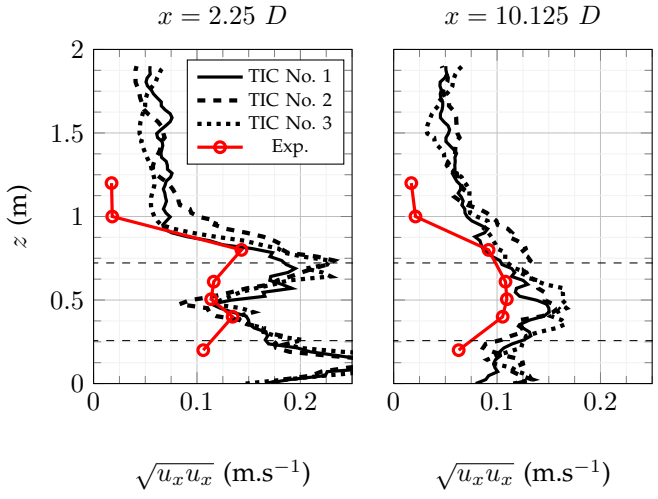

Fig. 16. Average velocity fluctuations $\sqrt{u_x u_x}$ at $x = 2.25\ D$ m and $10.125\ D$ downstream of the turbine. SEM used with TIC No. 1,2,3. Profiles are located at $y = 0.31$ m.

For further works it would be interesting to study the effect of the integral length scales based on the ratio length scale/turbine size. This could be done by studying a wider range of integral length scales or by changing the tidal turbine model scale. Moreover, a deeper knowledge of the spectral content of the turbulence generated by the SEM should be achieved in order to project the present study to real tidal sites.

Acknowledgement

The authors would like to thank Ifremer's Boulogne testing facility and HydroQuest® for sharing their experimental data with us. The present work was performed using computing resources of CRIANN (Normandy, France). This work is done in the framework of FCE INTERREG TIGER project.

References

[1] P. Mercier, M. Grondeau, S. Guillou, J. Thiébot, and E. Poizot, "Numerical study of the turbulent eddies generated by the seabed roughness. Case study at a tidal power site," vol. 97, Apr. 2020.

[2] P. Mycek, B. Gaurier, G. Germain, G. Pinon, and E. Rivaolen, "Experimental study of the turbulence intensity effects on marine current turbines behaviour. Part II: Two interacting turbines," *Renewable Energy*, vol. 68, pp. 876–892, 2014.

[3] T. Ebdon, M. J. Allmark, D. M. O'Doherty, A. Mason-Jones, T. O'Doherty, G. Germain, and B. Gaurier, "The impact of turbulence and turbine operating condition on the wakes of tidal turbines," *Renewable Energy*, vol. 165, pp. 96–116, Mar. 2021. [Online]. Available: https://linkinghub.elsevier.com/retrieve/pii/S0960148120318085

[4] M. Thiébaut, J.-F. Filipot, C. Maisondieu, G. Damblans, C. Jochum, L. F. Kilcher, and S. Guillou, "Characterization of the vertical evolution of the three-dimensional turbulence for fatigue design of tidal turbines," *Philosophical Transactions of the Royal Society A: Mathematical, Physical and Engineering Sciences*, vol. 378, no. 2178, p. 20190495, Aug. 2020. [Online]. Available: https://royalsocietypublishing.org/doi/10.1098/rsta.2019.0495

[5] U. Ahmed, D. D. Apsley, I. Afgan, T. Stallard, and P. K. Stansby, "Fluctuating loads on a tidal turbine due to velocity shear and turbulence: comparison of CFD with fields data," *Renewable Energy*, vol. 112, pp. 235–246, 2017.

[6] S. Shamsoddin and F. Porté-Agel, "Large Eddy Simulation of Vertical Axis Wind Turbine Wakes," *Energies*, vol. 7, pp. 890–912, 2014.

[7] Z. Guo and C. Shu, *Lattice Boltzmann Method and its Application in Engineering*. World Scientific, 2013.

[8] M. Grondeau, S. Guillou, P. Mercier, and E. Poizot, "Wake of a Ducted Vertical Axis Tidal Turbine in Turbulent Flows, LBM Actuator-Line Approach," *Energies*, vol. 12, no. 22, p. 4273, Nov. 2019. [Online]. Available: https://www.mdpi.com/1996-1073/12/22/4273

[9] M. Moreau, G. Germain, and G. Maurice, "Experimental performance and wake study of a ducted twin vertical axis turbine in ebb and flood tide currents at a 1/20th scale," *Renewable Energy*, p. S0960148123007589, Jun. 2023. [Online]. Available: https://linkinghub.elsevier.com/retrieve/pii/S0960148123007589

[10] P. F. Melani, F. Balduzzi, G. Ferrara, and A. Bianchini, "Tailoring the actuator line theory to the simulation of Vertical-Axis Wind Turbines," *Energy Conversion and Management*, vol. 243, p. 114422, Sep. 2021. [Online]. Available: https://linkinghub.elsevier.com/retrieve/pii/S0196890421005987

[11] S. Shamsoddin and F. Porté-Agel, "A large-eddy simulation of vertical axis wind turbine wakes in the atmospheric boundary layer," *Energies*, vol. 9, no. 366, pp. 1–23, 2016.

[12] J. Latt, O. Malaspinas, D. Kontaxakis, A. Parmigiani, D. Lagrava, F. Brogi, M. B. Belgacem, Y. Thorimbert, S. Leclaire, S. Li, F. Marson, J. Lemus, C. Kotsalos, R. Conradin, C. Coreixas, R. Petkantchin, F. Raynaud, J. Beny, and B. Chopard, "Palabos: Parallel Lattice Boltzmann Solver," *Computers & Mathematics with Applications*, vol. 81, pp. 334–350, Jan. 2021. [Online]. Available: https://linkinghub.elsevier.com/retrieve/pii/S0898122120301267

[13] J. Latt, "Lattice Boltzmann method with regularized pre-collision distribution functions," *Mathematics and Computers in Simulation*, vol. 72, pp. 165–168, Sep. 2006.
[14] O. Malaspinas and P. Sagaut, "Consistent subgrid scale modelling for lattice Boltzmann methods," *Journal of Fluid Mechanics*, 2012.
[15] R. Polleto, T. Craft, and A. Revell, "A new divergence free synthetic eddy method for the reproduction of inlet flow conditions for LES," *Flow, Turbulence and Combustion*, vol. 91, no. 3, pp. 519–539, 2013.
[16] M. Grondeau, J.-C. Poirier, S. Guillou, Y. Mear, P. Mercier, and E. Poizot, "Modelling the wake of a tidal turbine with upstream turbulence," *International Marine Energy Journal*, vol. 3, no. 2, pp. 83–89, Sep. 2020. [Online]. Available: https://www.marineenergyjournal.org/imej/article/view/56
[17] M. Grondeau, S. S. Guillou, J. C. Poirier, P. Mercier, E. Poizot, and Y. Méar, "Studying the Wake of a Tidal Turbine with an IBM-LBM Approach Using Realistic Inflow Conditions," *Energies*, vol. 15, no. 6, p. 2092, Mar. 2022. [Online]. Available: https://www.mdpi.com/1996-1073/15/6/2092
[18] A. J. Musker, "Explicit expression for the smooth wall velocity distribution in a turbulent boundary layer," *AIAA Journal*, vol. 17, no. 6, pp. 655–657, 1979.
[19] H. Xu and P. Sagaut, "Analysis of the absorbing layers for the weakly-compressible lattice Boltzmann schemes," *Journal of Computational Physics*, vol. 245, Mar. 2012.
[20] P. Bachant, A. Goude, and M. Wosnik, "Actuator line modeling of vertical-axis turbines," 2016, publisher: arXiv Version Number: 4. [Online]. Available: https://arxiv.org/abs/1605.01449